J Fluoresc (2011) 21:443–451
DOI 10.1007/s10895-010-0722-1

SHORT COMMUNICATION

Synthesis and Spectroscopic Study of Several Novel Annulated Azulene and Azafluoranthene Based Derivatives

P. Gąsiorski · K. S. Danel · M. Matusiewicz · T. Uchacz · R. Vlokh · A. V. Kityk

Received: 6 June 2010 / Accepted: 8 September 2010 / Published online: 1 October 2010

Abstract A series of cyclized five-membered annulated azafluoranthene (AAF) and seven-membered annulated azulene (AA) derivatives have been synthesized and characterized by spectroscopic methods. The optical absorption and fluorescence spectra have been recorded in organic solvents of different polarity and analyzed within the semiempirical quantum chemical model PM3. In combination with the molecular dynamics simulations it properly reproduces the overall shape of the measured absorption spectra of both AA and AAF dyes including the strongest band in the region of 250–300 nm and the broad first absorption band above 400 nm. While the solvent polarity rises all the dyes exhibit the hypsochromic shift of the first absorption band and the bathochromic shift of the fluorescence band. Such opposite solvatochromic trends appear to be consistent with the Lippert–Mataga solvatochromic model. Compared to AA compounds, both AAF dyes reveal much stronger solvatochromic shift and broadening of the fluorescence band likewise the relative decrease in quantum yield on rising solvent polarity what may be an evidence for the intramolecular charge transfer mechanism being involved into the fluorescence emission. Depending on solvent polarity AA and AAF dyes emit light in the green–yellow range of the visible spectra what may be of interest for potential luminescent or electroluminescent applications.

Keywords Annulated azafluoranthenes · Annulated azulenes · Optical absorption spectra · Fluorescence spectra

P. Gąsiorski · M. Matusiewicz · A. V. Kityk (✉)
Faculty of Electrical Engineering,
Częstochowa University of Technology,
Al. Armii Krajowej 17, 42-200, Częstochowa, Poland
e-mail: kityk@ap.univie.ac.at

K. S. Danel
Department of Chemistry, University of Agriculture,
Balicka str. 122, 30-149 Kraków, Poland

T. Uchacz
Department of Chemistry, Jagiellonian University,
ul. R. Ingardena 3, 30-060, Kraków, Poland

R. Vlokh
Institute of Physical Optics,
Dragomanova str. 23, 79005, Lviv, Ukraine

Introduction

The interest to low weight organic dyes is attracted much by their photo-physical properties in a context of broad range of optoelectronic applications as fluorescent dopants (emitters) of dye lasers [1, 2] or electroluminescent devices [3, 4]. For this reason the electronic states and transitions as well as their correlation with structural, environmental and chemical substitution effects appear in a scope of numerous experimental and theoretical studies where the optical methods are combined with quantum chemical modeling. Our previous studies have been concentrated mainly on pyrazoloquinoline (1H-Pyrazolo[3,4-b]quinoline, hereafter abbreviated as PQ) and its derivatives representing intensely fluorescing dyes in solutions, polymer matrixes or solid state with the quantum yield approaching the unity in many cases [5, 6]. However the color gamut of PQ emitters corresponds mainly to the blue range of the spectra [7–12] what considerably limits the range of their potential applications. For this reason

we recently started a new program focused on the synthesis of annulated analogues of azafluoranthene and heteroazulene representing cyclized five- or seven-membered regioisomeric products of the phenyl PQ derivatives [13]. The spectral investigations and photophysical properties of a few such compounds have been reported in several recent publications [14–16]. The cyclization of PQs into azafluoranthenes or heteroazulene is found to be accompanied by a significant red shift of the first optical absorption and fluorescence bands. While the solvent polarity rises all the dyes exhibit the hypsochromic (blue) shift of the first absorption band and the bathochromic (red) shift of the fluorescence band. These trends have been reproduced within the semiempirical calculations and may be interpreted by a specific orientation of the dipole moments in ground and excited states of molecules.

In this paper we report the spectroscopic study and photophysical properties of several newly synthesized annulated azulene (AA) and azafluoranthene (AAF) based derivatives. They may be given by the following chemical structures:

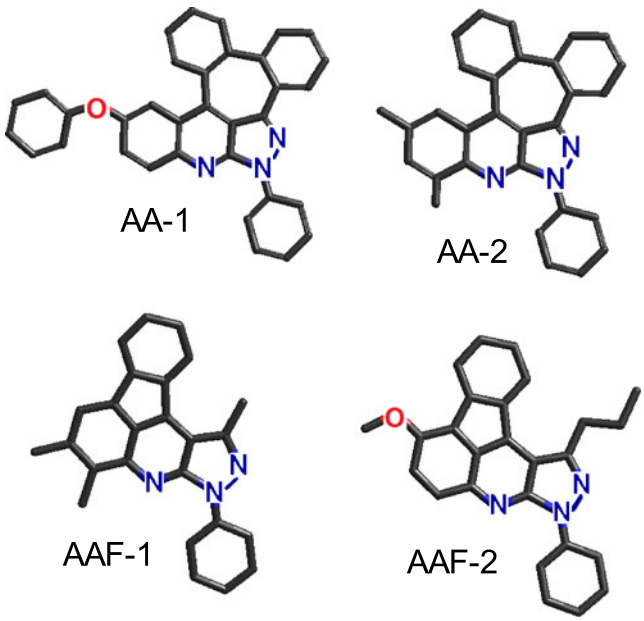

where the upper row of this scheme is represented by the cyclized seven-membered AA derivatives, 10-phenoxy-6-phenyl-*6H*-5,6,7-triazadibenzo[*f,h*]naphtho [3,2,1-*cd*]azulene and 8,10-dimethyl-6-phenyl-*6H*-5,6,7-triazadibenzo[*f,h*]naphtho[3,2,1-*cd*]azulene referenced hereafter as compounds AA-1, AA-2, respectively. Its second row presents two cyclized five-membered AAF derivatives, 1,5,6-trimethyl-3-phenyl-*3H*-indeno[1,2,3-*de*]pyrazolo[3,4-*b*]quinoline and 7-methoxy-3-phenyl-1-propyl-*3H*-indeno[1,2,3-*de*]pyrazolo[3,4-*b*]quinoline, referenced hereafter as compounds AAF-1 and AAF-2, correspondingly. By means of the optical absorption and fluorescence measurements we characterize here the electronic structure of these dyes and especially its modification due to solute-solvent interaction. For this reason the optical absorption and fluorescence spectra have been recorded in solvents of different polarity and consequently subjected to the quantum chemical analysis performed within the semiempirical method PM3.

Synthesis

Both AAs and AAFs may be easily obtained from the PQs according to the procedure described in [13], see also scheme below. To synthesize the seven-membered (AA) compounds the PQ starter (R_3 = Ph, X = Cl, Br) has been heated to reflux in (izo)quinoline in a presence of powdered KOH until digestion of the substrate. The palladium annulation reaction of PQs (X = Br) leads to five-membered (AAF) analogues in milder reaction conditions.

10-phenoxy-6-phenyl-*6H*-5,6,7-triazadibenzo[*f,h*]naphtho[3,2,1-*cd*]azulene (AA-1). Orange crystals; Mp = 73–75 °C; ^{1}H NMR ($CDCl_3$, 300 MHz) δ 7.05 (d, 2H, J = 8.4 Hz), 7.10 (t, 1H, J = 7.2 Hz), 7.22–7.44 (m, 7H), 7.51 (dd, 1H, J = 9.3, 2.7 Hz), 7.55 (t, 2H, J = 7.2 Hz), 7.65 (dd, 1H, J = 8.1, 1.5 Hz), 7.72–7.76 (m, 1H), 7.77 (dd, 1H, J = 7.8, 1.5 Hz), 7.93 (d, 1H, J = 2.4 Hz), 8.14 (d, 1H, J = 9.3 Hz), 8.27-8.30 (m, 1H), 8.57 (d, 2H, J = 8.7 Hz); Anal. Calcd. for $C_{34}H_{21}N_3O$; C, 83.76; H, 4.34; N, 8.62. Found: C, 83.65; H, 4.81; N, 8.46.

8,10-dimethyl-6-phenyl-*6H*-5,6,7-triazadibenzo[*f,h*]naphtho[3,2,1-*cd*]azulene (AA-2). Orange powder; Mp = 225–227 °C; ^{1}H NMR ($CDCl_3$, 300 MHz) δ 2.48 (d, 3H, J = 0.3 Hz, Me), 2.86 (s, 3H, Me), 7.27 (t, 1H, J = 7.5 Hz), 7.36–7.50 (m, 5H), 7.56 (t, 2H, J = 7.2 Hz), 7.71 (dd, 1H, J = 7.8, 1.5 Hz), 7.77–7.82 (m, 1H), 7.86 (dd, 1H, J = 7.8, 1.5 Hz), 8.06 (s, 1H), 8.27–8.36 (m, 1H), 8.71 (d, 2H, J = 8.9 Hz); Anal. Calcd. for $C_{30}H_{21}N_3$; C, 85.08; H, 5.00; N, 9.92. Found: C, 84.87; H, 5.09; N, 10.01.

1,5,6-trimethyl-3-phenyl-*3H*-indeno[1,2,3-*de*]pyrazolo[3,4-*b*]quinoline (AAF-1). Yellow powder; Mp = 220–222 °C; ^{1}H NMR ($CDCl_3$, 300 MHz) δ 2.46 (d, 3H, J = 0.3 Hz, Me), 2.71 (s, 3H, Me), 2.98 (s, 3H, Me), 7.28 (td, 2H, J = 7.5, 1.2 Hz), 7.38 (td, 1H, J = 7.5, 0.9 Hz), 7.45 (s, 1H), 7.56 (t, 2H, J = 7.5 Hz), 7.71 (ddd, 1H, J = 7.5, 0.9, 0.6), 8.08 (ddd, 1H, J = 7.5, 0.9, 0.6 Hz), 8.58 (d, 2H, J = 8.7 Hz); Anal. Calcd. for $C_{25}H_{19}N_3$; C, 83.08; H, 5.30; N, 11.63. Found: C, 82.95; H, 5.48; N, 11.45.

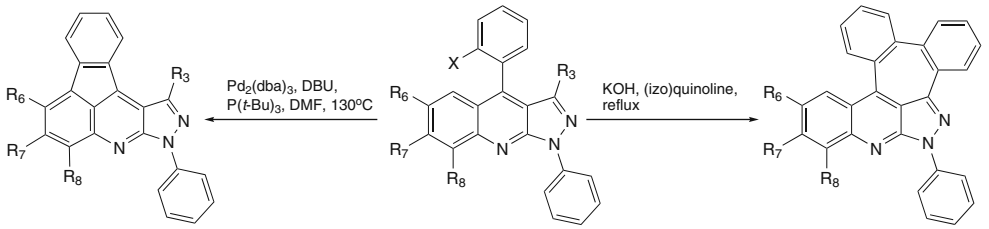

AA1: R_6 = OPh, R_7 = R_8 = H

AA2: R_6 = Me, R_7 = H, R_8 = Me

AAF-1: R_3 = Me, R_6 = H, R_7 = R_8 = Me

AAF-2: R_3 = n-Pr, R_6 = OMe, R_7 = R_8 = H

7-methoxy-3-phenyl-1-propyl-*3H*-indeno[1,2,3-*de*]pyrazolo[3,4-*b*]quinoline (AAF-2). Orange powder; Mp = 174–176 °C; ^{1}H NMR ($CDCl_3$, 300 MHz) δ 1.16 (t, 3H, $J = 7.5$ Hz), 2.00 (sextet, 2H, $J = 7.5$ Hz), 3.29 (t, 2H, $J = 7.5$ Hz), 4.04 (s, 3H, OMe), 7.25–7.35 (m, 3H), 7.40 (td, 1H, $J = 7.2$, 0.9 Hz), 7.56 (t, 2H, $J = 7.5$ Hz), 7.83 (d, 1H, $J = 9.3$ Hz), 7.98 (d, 2H, $J = 7.5$ Hz), 8.49 (d, 2H, $J = 8.7$ Hz); Anal. Calcd. for $C_{26}H_{21}N_3O$; C, 79.77; H, 5.41; N, 10.73. Found: C, 79.60; H, 5.48; N, 10.66.

Experimental and Calculation Procedures

The optical absorption spectra have been measured by means of the scanning spectrophotometer UV-VIS 2101 (Shimadzu) in the range of 230–600 nm. The steady state fluorescence was excited at the wavelength $\lambda_{ex} = 365$ nm and detected in a single photon counting mode using a conventional spectrofluorimeter supplied with the cooled photomultiplier EMI 955 8B. The spectral resolution in optical absorption or fluorescence meaurements was about 0.1 nm. The fluorescence spectra were corrected on the spectral sensitivity of the detecting system. The quantum yield was determined in steady-state measurements using the quinine sulphate in 0.05M H_2SO_4 solution as an actinometer. The fluorescence lifetime was determined by analyzing the temporal decay of the fluorescence spectra being excited by the picosecond diode laser from IBH-UK ($\lambda = 400$ nm, $\tau = 70$ ps pulse duration) and detected in a time-resolved single photon counting mode. The samples were prepared in the darkness and degassed before each measurement using the freezing-pumping-thawing technique. Both the optical absorption and fluorescence spectra were measured at room temperature in cyclohexane (CHX), tetrahydrofuran (THF) and acetonitrile (ACN) solutions with the molar concentration of the AA or AAF dyes of about 10^{-5} M in each case.

The quantum chemical analysis has been performed by means of the semiempirical method PM3 available in the quantum chemical package HyperChem-8.0. The geometrical optimization of the molecular structure in the ground state, molecular dynamics (MD) simulations as well as the calculations of the transition and state dipole moments have been performed using the same Hamiltonian, i.e. PM3 in each particular case. The electron correlation was accounted via the configuration interactions (CI) limited by a consideration of 30 occupied and 30 unoccupied orbitals. The optical absorption spectra have been calculated according to the procedure described in [17–20]. The MD trajectory has been generated in each particular case within the standard MD procedure at the simulation temperature $T = 300$ K and consisted of 200 consequent instantaneous conformations separated by a temporal interval of 0.5 ps. The optical absorption spectrum is an average over the spectra obtained within the consequent single point calculations. For each particular conformation of such MD trajectory the band shape of the simulated optical absorption spectra was defined by the Gaussian function, i.e. the molar extinction coefficient (m.e.c.) is $\propto f_i \exp\{2.773[(h\nu - \Delta E_i)/\Gamma]^2\}$, where $f_i \propto \Delta E_i |\mu_i^{(t)}|^2$ and ΔE_i are the oscillator strength and the energy of the electronic transition from the singlet ground state to ith excited singlet state, respectively, $\mu_i^{(t)}$ is the transition dipole moment of that electronic transition, h is the Planck constant, Γ is the empirical model parameter describing the Gaussian lineshape broadening.

Experimental Results and Discussion

Figure 1a–d show the steady-state optical absorption spectra of the AA and AAF dyes measured in CHX (blue online color) and ACN (red online color) solutions. In the range of 220–500 nm the spectra of these derivatives are characterized by several broad bands with the most strongest ones in the region of 250–270 nm. AA-1, AA-2 and AAF-1 dyes reveal the first absorption band in the region of 440–460 nm being slightly structured due to vibronic coupling. Similarly, AAF-2 dye is characterized by a broad but more evidently structured first absorption band with a maximum in the region of 476–482 nm. While the solvent polarity rises from CHX to ACN the absorption threshold of both AA and AAF dyes undergoes a weak blue shift what appears to be consistent with our recent spectroscopic studies on several other AA and AAF derivatives, see e.g. [14–16].

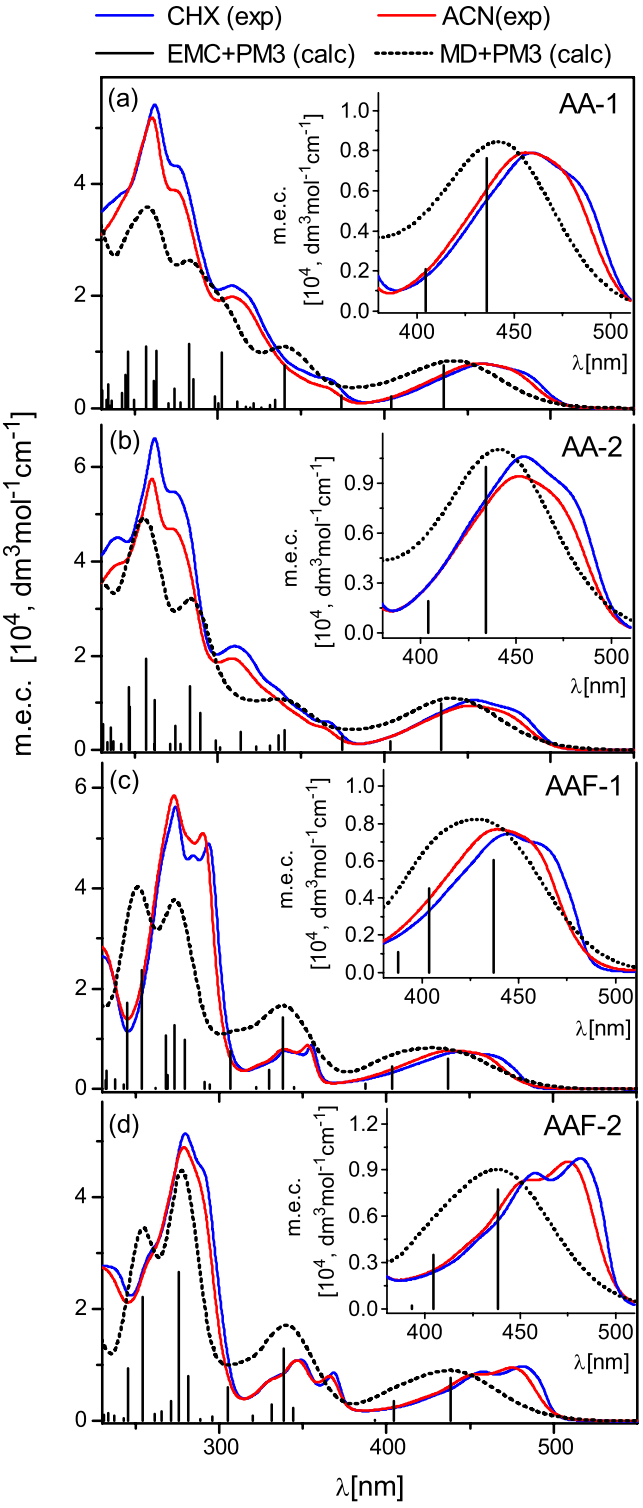

◀ **Fig. 1** The steady state optical absorption spectra of the AA and AAF dyes measured in CHX (*blue online color*) and ACN (*red online color*) solutions. *Vertical lines* (*black online color*) are the electronic spectra calculated by PM3 method for the EMC (PM3+EMC) in vacuo ($T = 0$ K, $\Gamma = 0$). The *continuous dot lines* (*black online color*) are the optical absorption spectra in the gas phase being calculated by PM3 method in combination with the MD simulations (PM3+MD) at T =300 K ($\Gamma = 0.3$ eV). **a** AA1 dye; **b** AA2 dye; **c** AAF1 dye; **d** AAF2 dye. The inserts in the sections **a**–**d** show the region of the first absorption band in details

Figure 2a–d show the normalized steady-state fluorescence spectra of the AA and AAF dyes measured in CHX (blue online color), THF (green online color) and ACN (red online color) solutions. For all the studied organic compounds the fluorescence bands are unstructured in most cases. Exceptions constitute only the fluorescence spectra of both AAF dyes measured in a weakly polar CHX solution. In contrast to the optical absorption the fluorescence exhibits a red shift while the solvent polarity changes from CHX to ACN. More evidently it is observed for the AAF derivatives where corresponding solvatochromic shift is accompanied by a significant broadening of the fluorescence bands in highly polar solvents. Our recent spectral investigations [14–16] show that stronger solvatochromism is typical also for other AAF dyes.

Table 1 lists the optical absorption and fluorescence maxima obtained in solvents of different polarity together with other photophysical characteristics. The quantum yield Φ_f, fluorescence lifetime τ_f, radiative (k_f) and radiationless (k_n) rate constants as well as the fluorescence moment M_f have been evaluated within a simple kinetic model of an irreversible excited charge transfer state [21]. One can see that the fluorescence efficiency decreases for all the dyes in strongly polar solvents, however the relative changes in Φ are considerably larger for the AAF dyes. On the other hand, the strongest quantum yield (Φ_f =94 %) is found for AA-1 in CHX solution. All the derivatives demonstrate

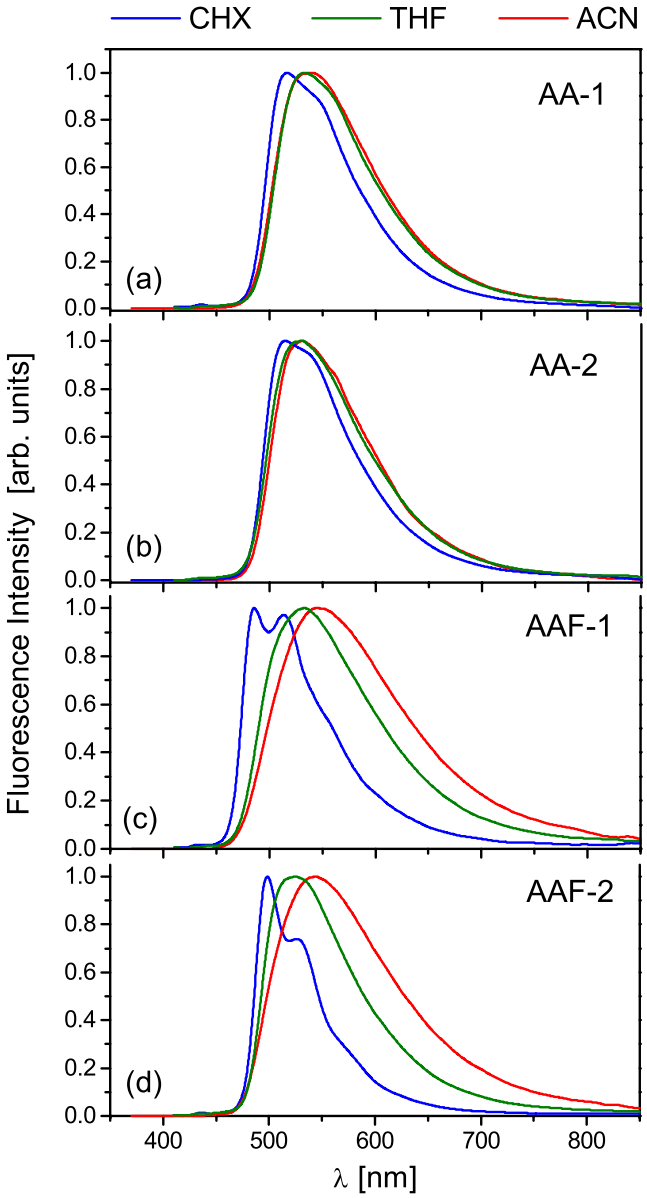

Fig. 2 The steady state normalized photoluminescence spectra of the AA and AAF dyes measured in CHX (*blue online color*), THF (*green online color*) and ACN (*red online color*) solutions. **a** AA1 dye; **b** AA2 dye; **c** AAF1 dye; **d** AAF2 dye

rather similar values of the fluorescence momentum in different solvents. The magnitude of M_f decreases here less than 20% while the solvent polarity changes from CHX to ACN.

In the following we analyze the measured optical absorption spectra and solvatochromic shifts within the semiempirical quantum chemical model PM3. The geometry optimization leads to the equilibrium conformations as shown in Fig. 3. Both types of derivatives are characterized by several equilibrium molecular geometries with nearly the same total energy. Corresponding equilibrium states differ from each other mainly by an angular orientation of the phenyl ring defined via the bond torsion angle N-N-C-C. For the AAFs the phenyl moiety appears in a symmetric double-well potential with the equilibrium torsion angles ±20.9 deg and ±22.1 deg as for AAF-1 and AAF-2, respectively. Contrary to this, the phenyl ring of the AAs is characterized by an essentially asymmetric potential with the equilibrium torsion angles 46.3 and −15.1 deg (AA-1) or 40.7 and −12.7 deg (AA-2), respectively. Such asymmetry is obviously related with a specific geometry of phenyl-azulene moiety being substantially bent in the ground state as one can see in Fig. 3. For comparison, the phenyl-azafluoranthene moiety of AAFs is perfectly flat. However, it is more important that the equilibrium angular states in both AAs and AAFs are found to be separated by relatively small energy barriers being comparable or much less than the thermal energy $k_B T$ at $T = 300$ K. This leads to quite large libration amplitudes of the rotating phenyl ring, even up to about ±40 deg. For this reason the semiempirical calculations of the electronic spectra are combined in the current study with the MD simulations. The vertical lines (black online color) in Fig. 1a–d represent the electronic spectra calculated by PM3 method for the equilibrium molecular conformation (EMC) in vacuo (referred hereafter as PM3+EMC) at $T = 0$ K and $\Gamma = 0$. The continuous dot lines (black online color) are the optical absorption spectra in the gas phase being calculated by PM3 method in combination with the MD simulations (referred hereafter as PM3+MD) at $T = 300$ K ($\Gamma = 0.3$ eV). One can realize that quantum chemical calculations in combination with MD simulations quite properly reproduce the overall shape of the absorption spectra including the strongest band(s) in the region of 250–300 nm and the broad first absorption band which occurs above 400 nm. However, more detailed comparison of the measured and calculated spectra indeed reveals a difference in the spectral position of the first absorption band. For all the dyes the semiempirical calculations give the absorption threshold position somewhat blue shifted comparing to the measured ones. However, for most dyes this difference appears to be less than 0.1 eV. Only for AAF-2 the evaluated absorption threshold position is characterized by a larger error, ∼0.2 eV. The observed discrepancies should not be attributed to the precision of the semiempirical calculations only but are also related with an ignoring of solvent effects during the calculation.

A challenging question remains an opposite solvatochromic behavior of the first absorption and fluorescence bands. We interpret this within the

Table 1 The photophysical constants of AA and AAF dyes in different solutions

Compound	Solvent	λ_m^a [nm]	λ_m^f [nm]	Φ_f	τ_f [ns]	k_n [10^7, s^{-1}]	k_f [10^7, s^{-1}]	M_f [D]
AA-1	CHX	460.0	517.0	0.940	17.8	0.34	5.3	2.83
	THF	458.5	533.0	0.722	18.8	1.5	3.8	2.59
	ACN	457.0	538.5	0.713	19.5	1.5	3.7	2.73
AA-2	CHX	454.5	515.0	0.51	16.3	3.0	3.1	2.17
	THF	453.0	526.0	0.53	17.2	2.7	3.1	2.27
	ACN	452.0	531.0	0.41	18.6	3.2	2.2	2.08
AAF-1	CHX	445.5	498.0	0.16	8.3	10.1	1.9	1.62
	THF	441.0	530.0	0.076	7.3	12.7	1.0	1.34
	ACN	439.0	547.0	0.051	4.8	19.8	1.1	1.51
AAF-2	CHX	482.0	499.0	0.4	9.4	6.4	4.3	2.41
	THF	480.0	524.5	0.228	9.5	8.1	2.4	2.0
	ACN	476.0	541.0	0.098	5.0	18.0	2.0	2.02

λ_m^a is the absorption maxima, λ_m^f is the fluorescence maxima, Φ_f is the fluorescence quantum yield, τ_f is the fluorescence lifetime, k_n is the radiationless rate constant, k_f is the radiative rate constant and M_f is the fluorescence moment

Lippert–Mataga dielectric polarization model [22, 23] describing the solvent modified wavenumbers of the optical absorption ($\nu^a = 1/\lambda_m^a$) or fluorescence ($\nu^f = 1/\lambda_m^f$) maxima as:

$$\nu^a = \nu_0^a - 2\boldsymbol{\mu}_g\left(\boldsymbol{\mu}_e - \boldsymbol{\mu}_g\right) F(\varepsilon, n)/\left(hca_0^3\right) \quad (1)$$

$$\nu^f = \nu_0^f - 2\boldsymbol{\mu}_e\left(\boldsymbol{\mu}_e - \boldsymbol{\mu}_g\right) F(\varepsilon, n)/\left(hca_0^3\right) \quad (2)$$

where $F(\varepsilon, n) = (\varepsilon - 1)/(2\varepsilon + 1) - (n^2 - 1)/(4n^2 + 2)$ is the polarity function of the solvent being defined by its refractive index n and static dielectric constant ε, ν_0^a and ν_0^f are the spectral positions of the absorption and fluorescence maxima in the gas phase, respectively, c is the light speed, a_0 is the Onsager (cavity) radius, $\boldsymbol{\mu_g}$ and $\boldsymbol{\mu_e}$ are the ground and excited state dipole moments, respectively. Accordingly, the type of solvatochromism (hypsochromic or bathochromic) likewise its strength are in fact defined by the signs and magnitudes of the solvatochromic factors $\boldsymbol{\mu}_g(\boldsymbol{\mu}_e - \boldsymbol{\mu}_g)$ and $\boldsymbol{\mu}_e(\boldsymbol{\mu}_e - \boldsymbol{\mu}_g)$. Table 2 presents their magnitudes determined from the measured spectra and evaluated within the semiempirical model via the calculated state dipole moments $\boldsymbol{\mu_g}$ and $\boldsymbol{\mu_e}$. The quantum chemical calculations result for all the dyes to a proper signs of the solvatochromic shift what in fact appears to be a sequence of a specific spatial orientation of the dipole moments $\boldsymbol{\mu}_g$ and $\boldsymbol{\mu}_e$. Comparing the calculated and measured solvatochromic slopes of the first optical absorption band, being defined by the factor $\boldsymbol{\mu}_g(\boldsymbol{\mu}_e - \boldsymbol{\mu}_g)/a_0^3$, one must also pay attention on rather good quantitative agreement. However, this is not the case in respect to other factor, $\boldsymbol{\mu}_e(\boldsymbol{\mu}_e - \boldsymbol{\mu}_g)/a_0^3$, which defines the solvatochromic shift of the fluorescence band. The quantitative discrepancy between the experiment and theory is here about one order of magnitude. The experiment reveals much stronger solvatochromic red shift indicating thus on considerably larger dipole moment $|\boldsymbol{\mu}_e|$ of the excited state being involved into a fluorescence emission. In regard to this several possible reasons should be mentioned:

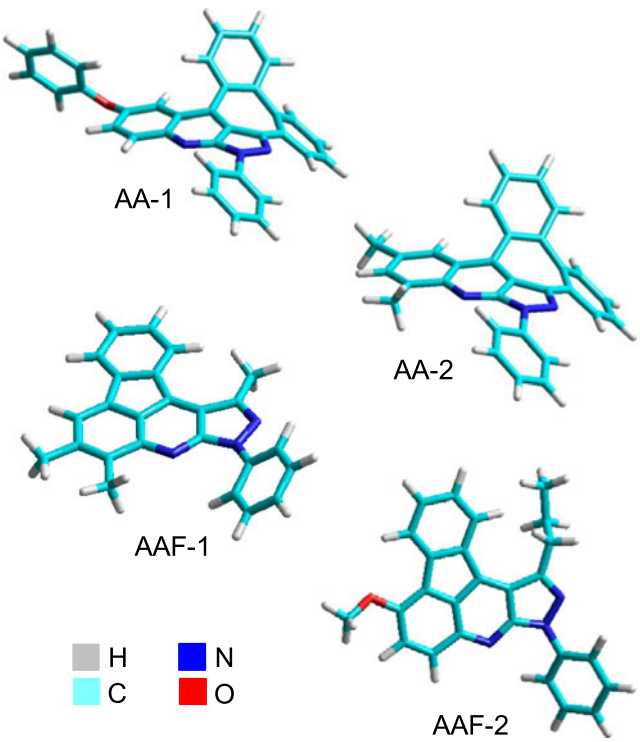

Fig. 3 The ground state EMC structure of the AA and AAF dyes in vacuo (gas phase) as obtained within the optimization procedure by the quantum chemical method PM3

i) The dipole moments have been calculated in the gas phase, i.e. as for the ground state equilibrium molecular geometry in vacuo ignoring any solvation effects. To treat the problem properly, a program which includes the solvation energy in the Hamiltonian should be used.
ii) The quantum chemical analysis ignores the Franck-Condon relaxation of molecular structure

Table 2 Solvatochromic factors for AA and AAF dyes as determined from optical absorption and fluorescence measurements and calculated within the semiempirical model PM3

Compound		$\boldsymbol{\mu}_g(\boldsymbol{\mu}_e - \boldsymbol{\mu}_g)/a_o^3$ [eV]	$\boldsymbol{\mu}_e(\boldsymbol{\mu}_e - \boldsymbol{\mu}_g)/a_o^3$ [eV]
AA-1	Exp.	−0.029	0.164
	PM3+EMC (Calc.)	−0.032	0.026
	PM3+MD (Calc.)	−0.035	–
AA-2	Exp.	−0.0248	0.124
	PM3+EMC (Calc.)	−0.046	0.012
	PM3+MD (Calc.)	−0.055	–
AAF-1	Exp.	−0.071	0.377
	PM3+EMC (Calc.)	−0.067	0.041
	PM3+MD (Calc.)	−0.05	–
AAF-2	Exp.	−0.055	0.320
	PM3+EMC (Calc.)	−0.062	0.036
	PM3+MD (Calc.)	−0.063	–

The Onsager radius a_0 scales according to the cube root of molecular volume and taken equal to 4.95, 4.77, 4.56 or 4.66 Å as for AA-1, AA-2, AAF-1 or AAF-2, respectively

in the excited state toward a new (equilibrium) conformation which may result to a substantial modification of the electronic transitions likewise the dipole moments of the excited states including the lowest one.

iii) In addition to the eventual solute relaxation, as mentioned in (ii), the solute-solvent interaction (solute in Onsager reaction field) lowers the energy of the excited states. The effect is considerably stronger for those excited states that are characterized by large state dipole moments, such as e.g. intramolecular charge transfer (ICT) states. A considerable lowering of their energies in a polar solvent environment may lead basically to the two cases. Either one of the strongly polar excited ICT states of the solute becomes in solvent the lowest excited singlet fluorescent state (so-called inversion of states) or the lowest locally excited (LE) weakly dipolar state appears to be strongly modified due to its mixing with strongly dipolar ICT states that just approach the LE state in polar solvent.

We favor the last case, especially for AAF dyes, taking into account that the fluorescence quantum yield (see Table 1) of these compounds reveals strong decrease if the solvent polarity rises from CHX to ACN. Following [24] such behavior is typical for many fluorescent materials. In the case of AAF dyes it may be explained by a stabilization of the ICT state at higher polar solvents, and emission from the LE state in lower-polarity solvents. Accordingly, a decrease in Φ is possible because the ICT emission is from a different electronic state than the LE emission. In other words, in highly polar solvents due to a considerable mixing of the LE and ICT states the lowest excited state of AAF dyes appears to be strongly modified and gets features mostly of ICT state, and vice versa. Lowering of ICT states in polar solvents activates radiationless transitions of AAF dyes (see Table 1) what is the reason for a considerable decrease in their fluorescence efficiency. Here basically two competitive mechanisms may be involved into the nonradiative depopulation of the lowest excited state: i) the intersystem crossing providing the population of the triplet states and ii) a direct radiationless charge recombination to the singlet ground (S_0) state [25]. However, the available data are not sufficient to make a conclusion which of these mechanisms is dominant. One should be emphasized, that a reduction in the quantum yield vs the rising solvent polarity is substantially stronger for AAF-1 or AAF-2 compared to the AA dyes. This finding quite well correlates with the larger solvatochromic red shift and broadening of the fluorescence band observed for both AAF dyes in the experiment (see Fig. 2). Thereby, it may be suggested that the red-shifted transition in AAF-1 and AAF-2 compounds is preferably due to ICT which is known to be affected by a solvent polarity. In contrast to this, both AA-1 and AA-2 dyes exhibit the excited fluorescent state which even in highly polar solvent environment still keeps characteristic features of the LE state.

The discussion presented above is relevant with the quantum chemical analysis. In particular, it shows that for the ground state geometry the next excited singlet state (S_2) of AAF dyes is indeed characterized by a better charge separation upon the excitation comparing to the lowest excited state S_1. This provides therefore a lager dipole moment $|\mu_2|$ for this state, 4.4 D and 7.0 D as for AAF-1 and AAF-2, respectively. The state S_2 may be considered therefore as moderately dipolar ICT state. Rotation of the phenyl ring towards planarity gives further rise of these dipole moments to 4.7 D and 7.5 D, correspondingly. Also the dipole moment of the lowest excited state S_1 exhibits lager magnitudes for the planar conformations. This finding suggests that in the polar solvents the AAF molecules after the excitation will tend to more planar geometries with simultaneous lowering of their state energies. Corresponding

energy shift ΔE for the state characterizing by the dipole moment $|\mu_i|$ can be evaluated within the polarization continuous model as for the point charge dipole in the reaction Onsager field, $\Delta E = -(|\mu_i|^2/a_0^3)(\varepsilon - 1)/(2\varepsilon + 1)$. Accordingly, due to a much stronger lowering of the state S_2 compared to the state S_1, the energy gap between them appears to be considerably reduced. In the ACN solution ($\varepsilon = 37.5$) our evaluation give its value even less than 0.17 or 0.09 eV, as for AAF-1 or AAF-2, respectively. For this reason the mixing of these states seems to be very likely in the highly polar solvents. Assuming that the ICT state S_2 would be the emission one it would be characterized also by a larger magnitude of the fluorescence solvatochromic shift $[\boldsymbol{\mu}_e(\boldsymbol{\mu}_e - \boldsymbol{\mu}_g)/a_0^3]$ being equal to about 0.07 eV (AAF-1) and 0.21 eV (AAF-2), i.e. in a better agreement with the experiment. One should be emphasized that the Onsager radius a_0 represents here a crude parameter of the model thus the evaluation given above should be rather considered as a rough estimation only. Nevertheless, the model presented above explains the most possible reason for the essential modification of the lowest excited state of AAF dyes in a polar environment. For comparison, the quantum chemical calculations of both AA dyes give the magnitudes of the dipole moment for the excited state S_2 less than 1.8 D. Thereby particularly this state, even in highly polar solvents, should not influence the lowest excited state S_1. A weak fluorescence solvatochromism demonstrating by AA-1 and AA-2 dyes remains to be relevant with a weakly dipolar character of their emission state S_1.

Conclusion

Taking together, a series of cyclized five-membered AAF and seven-membered AA derivatives have been synthesized and characterized by spectroscopic methods. The optical absorption spectra have been recorded in organic solvents of different polarity and analyzed within the semiempirical quantum chemical approach. The rotational dynamics of the phenyl groups is characterized in both AAs and AAFs by quite large angular amplitudes. For this reason the calculations of the optical absorbtion spectra have been performed by means of semiempirical method PM3 in combination with the MD simulations. Such hybrid model quite properly reproduces the overall shape of the absorption spectra of both AA and AAF dyes including the strongest band(s) in the region of 250–300 nm and the broad first absorption band which arises above 400 nm. While the solvent polarity changes from CHX to ACN all the dyes exhibit the hypsochromic shift of the first absorption band and the bathochromic shift of the fluorescence band. These findings appear to be consistent with the Lippert–Mataga solvatochromic model. The different solvatochromic trends in a spectral position of the optical absorbtion and fluorescent bands are explained by specific orientations of the ground and excited state dipole moments. However, the semiempirical calculations give quite reasonable magnitude of the solvatochromic shift concerning the first absorption band only. Regarding the fluorescence spectra the experiment indicates on a considerably larger dipole moment of the excited state(s) involved into a fluorescence emission. As possible reasons for such discrepancy may be geometrical relaxation of the molecules in the excited state likewise a mixing of the weakly dipolar LE state with the strongly dipolar ICT states energy of which lowers in polar solvent environment. Corresponding effects appear to be much evident for the AAF dyes which are characterized in highly polar solvents by a stronger relative changes in quantum yield correlating with a larger solvatochromic red shift of the emission band likewise its evident broadening. Depending on solvent polarity the AA and AAF dyes emit light in the green–yellow range of the visible spectra what may be of interest for luminescent or electroluminescent applications. The quantum yield of these dyes considerably rises in a weakly polar environment.

References

1. Speiser S, Shakkour N (1985) Photoquenching parameters for commonly used laser-dyes. Appl Phys B 38:191–197
2. Tu J, Li N, Chi Y, Qu S, Wang C, Yuan Q, Li X, Qiu S (2009) The study of photoluminescence properties of Rhodamine B encapsulated in mesoporous silica. Mater Chem Phys 118:273–276
3. Całus S, Gondek E, Danel A, Jarosz B, Pokladko M, Kityk AV (2007) Electroluminescence of 6-R-1,3-diphenyl-1H-pyrazolo[3,4-b]quinoline-based organic light-emitting diodes (R = F, Br, Cl, CH_3, C_2H_3 and $N(C_6H_5)_2$). Mater Lett 61:3292–3295
4. Gondek E, Całus S, Danel A, Kityk AV (2008) Photoluminescence and electrolurninescence of methoxy and carboethoxy derivatives of 1,3-diphenyl-1H-pyrazolo[3,4-b] quinoline. Spectrochim Acta Part A 69:22–26
5. Rechthaler K, Rotkiewicz K, Danel A, Tomasik P, Khatchatryan K, Köhler G (1997) Emissive properties and intramolecular charge transfer of pyrazoloquinoline derivatives. J Fluoresc 7:301–309
6. Parusel ABJ, Rechthaler K, Piorun D, Danel A, Khatchatryan K, Rotkiewicz K, Köhler G (1998) Fluorescence properties of donor-acceptor-substituted pyrazoloquinolines. J Fluoresc 8:375–387
7. Całus S, Gondek E, Danel A, Jarosz B, Nizioł J, Kityk AV (2007) Photoluminescence of methoxy and carboethoxy

derivatives of 1,3-diphenyl-1H-pyrazolo[3,4-b]quinoline: experiment and quantum-chemical simulations. Mater Sci Eng B 137:255–262
8. Całus S, Gondek E, Danel A, Jarosz B, Kityk AV (2007) Photoluminescence of 1,3-Diphenyl-1H-pyrazolo[3,4-b]quinoline and its derivatives: experiment and quantum chemical simulations. Opt Commun 271:16–23
9. Koścień E, Gondek E, Pokladko M, Jarosz B, Vlokh RO, Kityk AV (2009) Photoluminescence of 1,3-dimethyl pyrazoloquinoline derivatives. Mater Chem Phys 114:860–867
10. Gondek E, Danel A, Kwiecień B, Nizioł J, Kityk AV (2010) Photoluminescence spectra of bisphenol A based pyrazoloquinoline dimers in different solvents: experiment and quantum chemical calculations. Mater Chem Phys 119:140–144
11. Koścień E, Gondek E, Jarosz B, Danel A, Nizioł J, Kityk AV (2009) Photoluminescence of 1-phenyl,3-methyl pyrazoloquinoline derivatives. Spectrochim Acta Part A 72:582–590
12. Mac M, Uchacz T, Andrzejak M, Danel A, Szlachcic P (2007) Photophysical properties of some donor-acceptor 1H-pyrazolo[3,4-b]quinolines—radiative versus non-radiative electron transfer processes. J. Photochem Photobiol A 187: 78–86
13. Danel KS, Wisła A, Uchacz T (2009) Unexpected intramolecular cyclization of 4-(2-halophenyl)-1H-pyrazolo [3,4-b]quinolines: formation of 5-and 7-membered rings from one starter. ARKIVOC x:71–78
14. Całus S, Danel KS, Uchacz T, Kityk AV (2010) Optical absorption and fluorescence spectra of novel annulated analogues of azafluoranthene and azulene dyes. Mater Chem Phys 121:477–483
15. Danel KS, Gąsiorski P, Matusiewicz M, Całus S, Uchacz T, Kityk AV (2010) UV–vis spectroscopy and semiempirical quantum chemical studies on methyl derivatives of annulated analogues of azafluoranthene and azulene dyes. Spectrochim Acta Part A 77:16–23
16. Gąsiorski P, Danel KS, Matusiewicz M, Uchacz T, Kityk AV (2010) From pirazoloquinolines to annulated azulene dyes: UV–VIS spectroscopy and quantum chemical study. J Lumin. doi:10.1016/j.jlumin.2010.08.013
17. Koścień E, Sanetra J, Gondek E, Danel A, Wisła A, Kityk AV (2003) Optical absorption measurements and quantum-chemical simulations on 1H-pyrazolo[3,4-b]quinoline derivatives. Opt Commun 227:115–123
18. Gondek E, Koścień E, Sanetra J, Danel A, Wisla A, Kityk AV (2004) Optical absorption of 1H-pyrazolo[3,4-b]quinoline and its derivatives. Spectrochim Acta Part A 60:3101–3106
19. Koścień E, Sanetra J, Gondek E, Jarosz B, Kityk IV, Ebothe J, Kityk AV (2005) Optical poling effect and optical absorption of cyan, ethylcarboxyl and tert-buthyl derivatives of 1H-pyrazolo[3,4-b]quinoline: experiment and quantum-chemical simulations. Spectrochim Acta Part A 61:1933–1938
20. Całus S, Gondek E, Danel A, Jarosz B, Kityk AV (2006) Optical absorption of 1,3-diphenyl-1H-pyrazolo[3,4-b]quinoline and its derivatives. Opt Commun 268:64–74
21. Kapturkiewicz A, Herbich J, Karpiuk J, Nowacki J (1997) Intramolecular radiative and radiationless charge recombination processes in donor-acceptor carbazole derivatives. J Phys Chem A 101:2332–2344
22. Lippert E (1955) Dipolmoment und elektronenstruktur von angeregten molekulen. Z Naturforsch A10:541–545
23. Mataga N, Kaifu Y, Koizumi M (1955) The solvent effect on fluorescence spectrum—change of solute-solvent interaction during the lifetime of excited solute molecule. Bull Chem Soc Jpn 28:690–691
24. Lakowicz JR (2006) Principles of fluorescence spectroscopy, 3rd edn. Springer, 953 pp
25. Kapturkiewicz A, Nowacki J (1999) Properties of the intramolecular excited charge-transfer states of carlbazol-9-yl derivatives of aromatic ketones. J Phys Chem A 103:8145–8155